Metal-dielectric-metal resonators with deep subwavelength dielectric layers increase the near-field SEIRA enhancement

Jungseok Chae,[1,2] Basudev Lahiri,[1,2] John Kohoutek,[1,2] Glenn Holland,[1] Henri Lezec[1] and Andrea Centrone[1*]

[1]*Center for Nanoscale Science and Technology, National Institute of Standard and Technology, Gaithersburg, MD 20899, USA*

[2]*Maryland Nanocenter, University of Maryland, College Park, MD 20742, USA*

[*]*andrea.centrone@nist.gov*

Abstract: Plasmonic nanostructures presenting either structural asymmetry or metal-dielectric-metal (M-D-M) architecture are commonly used structures to increase the quality factor and the near-field confinement in plasmonic materials. This characteristic can be leveraged for example to increase the sensitivity of IR spectroscopy, via the surface enhanced IR absorption (SEIRA) effect. In this work, we combine structural asymmetry with the M-D-M architecture to realize Ag-Ag_2O-Ag asymmetric ring resonators where two Ag layers sandwich a native silver oxide (Ag_2O) layer. Their IR response is compared with the one of fully metallic (Ag) resonators of the same size and shape. The photothermal induced resonance technique (PTIR) is used to obtain near-field SEIRA absorption maps and spectra with nanoscale resolution. Although the native Ag_2O layer is only 1 nm to 2 nm thick, it increases the quality factor of the resonators' dark-mode by ≈ 27 % and the SEIRA enhancement by ≈ 44 % with respect to entirely Ag structures.

1. Introduction

Metamaterials are artificially engineered materials that exhibit peculiar electromagnetic properties such as negative refraction [1], artificial magnetism [1] and symmetry breaking absorption [2]. These properties are leveraged for important applications such as sensing [3-5], photovoltaics [6, 7], cloaking [8], etc. Metallic split ring resonators are a class of metamaterials [9-12] whose characteristic optical resonant response, hereafter surface plasmon resonance (SPR), can be tuned from the terahertz to the visible spectral regions [9, 11, 13, 14]. In particular, the recent development of plasmonic nanostructures with resonances in the mid-infrared has generated considerable interest in surface-enhanced infrared absorption (SEIRA) spectroscopy [5, 15-23], due to chemical detection limits in the zeptomolar range [5]. Resonators with high quality factors (Q), defined as the ratio of the SPR peak wavelength to its full width half maximum, are desirable for sensing applications because peak shifts induced by analyte adsorption are more easily detected on sharp peaks and because the resonant enhancement of the local optical field intensity is proportional to Q^2 [24]. However, the strong coupling between light and the SPRs in the visible and infrared (IR) regions give rise to significant radiation losses in the resonators, [13, 25] that combined with the metamaterials absorption losses, de facto limit the quality factors in plasmonic materials [13, 25]. Despite these limitations, the strong mode confinement in the resonators' near-field compensates the low Q and typically results in better detection sensitivity than alternative technology such as photonic crystals and resonators [24]. Consequently, improving the Q-factor and the mode confinement in plasmonic materials is important for improving the performance of metamaterials in sensing applications.

One approach to increase Q in these materials relies on asymmetric structures like the asymmetric split ring resonators (ASRRs) [13, 25-27]. ASRRs are plasmonic structures

composed by two metallic arcs of different length sharing the same center of curvature. In ASRRs the fundamental plasmonic modes of the two arcs hybridize, forming symmetric ("bright") and anti-symmetric ("dark") collective modes. The interference of the broader "bright" mode with the narrower "dark" mode [7, 28] leads to Fano-shaped peaks that are sharper and have better Q than their symmetric counterparts because the dark-mode reduces the coupling with the free space and lowers the scattering losses [13, 25-27]. Another, less explored approach to increase the resonators sensitivity relies on metal-dielectric-metal (M-D-M) sandwich structures [29-33] as a mean to increase the plasmonic mode confinement and the enhancement in the near-field. For example, it was reported [29] that a very thin oxide layer sandwiched between silver films can increase the surface enhanced Raman scattering (SERS) signal up to 10 times with respect to bare silver films. Also, theoretical calculations predicted larger near-field enhancements for nanocrescents [30], bow ties [31], nanorods [32] and cross-shaped nanobars [33] made by M-D-M structures with a silica core with respect to fully metallic structures of the same size. Similar single or multi-layered M-D-M structures such as fishnet [34], nanorods [35] and stacked plasmonic waveguides [36] have been known to exhibit negative refraction at optical frequencies.

In this work, the SEIRA enhancement in polymer films surrounding M-D-M ASRR structures is measured with nanoscale resolution using the photo-thermal induced resonance (PTIR) technique, [37, 38] a novel method that combines the lateral resolution of atomic force microscopy (AFM) with the chemical specificity of infrared (IR) spectroscopy. M-D-M ASRR structures consisting of two Ag layers sandwiching a very thin dielectric layer of native silver oxide (Ag_2O) are compared with entirely metallic (Ag) ASRR structures of the same size and shape. Results show that the near-field enhancement is up to 44 % stronger in the M-D-M ASRRs than in all silver reference structures. Because the resonant wavelength of the resonators analyzed here is ≈ 8.6 μm and the thickness of the native silver oxide is in the order of 1 nm to 2 nm [39, 40], the deeply subwavelength (between ≈ λ/4300 and ≈ λ/8600) dielectric layer in these structures has an pronounced effect on the field localization and enhancement.

2. Fabrication and measurements

To enable PTIR characterization the ASRR arrays were fabricated on a Zinc Selenide (ZnSe) right-angle prisms by a combination of electron beam lithography and metal lift-off techniques (see Fig. 1) using custom adaptor pieces described elsewhere [37].

Two resonators arrays were fabricated: i) an ASRR array with resonators made entirely by Ag (hereafter, ASRR-Ag) was used as a reference and ii) an ASRR array where a thin native Ag oxide (Ag_2O) dielectric layer is sandwiched between two Ag layers (hereafter, ASRR-Ag-Ag_2O-Ag) was used to evaluate the effect of the dielectric layer on the near-field enhancement. The ASRR-Ag-Ag_2O-Ag sample was fabricated by exposing the bottom Ag layer (thickness ≈ 85 nm) to air for 48 h before depositing the top Ag layer (thickness ≈ 85 nm). We choose 48 h of air exposure because it was previously found [29] that this is the optimal time to maximize the SERS enhancement in Ag M-D-M films. Care was taken to avoid exposing the samples studied here to a sulfur sources which may cause formation of a silver sulphide layer [40]. The two resonators samples have the same nominal dimensions (external diameter ≈ 1.75 μm, pitch ≈ 3.0 μm, thickness ≈ 170 nm). Figure 2 shows AFM images of fabricated resonator arrays; the effective resonator dimensions were measured by AFM and are summarized in Table 1. Although the thickness of the native oxide layer growing on silver when exposed to air is limited to 1 nm or 2 nm [39, 40], it is sufficient to enhance the resonators quality factor and near field enhancement (see below).

Far-field Fourier transform infrared (FTIR) reflectance spectra were recorded with an FTIR spectrometer interfaced with an infrared microscope equipped with a 36x reverse Cassegrain reflection objective (NA = 0.52) and a ZnSe wire grid polarizer (to control the light polarization). The spectra were collected through an aperture window of 150 μm x 150 μm

which allowed sampling the response of approximately 2,500 resonators in each spectrum. 128 spectra (4 cm^{-1} resolution) were acquired and averaged for each sample. The FTIR reflectance spectra (Fig. 3) were recorded with linearly polarized light with the electric field parallel to the long direction of the arcs (parallel polarization). The spectra show plasmonic peaks with the characteristic Fano-shaped profile due to interference between the bright and dark modes of the resonators [3]. The resonance frequencies and Q-factors of bright and dark modes are obtained by the fitting the FTIR spectral profile with analytical Fano intereference model [41, 42]:

$$s(\omega) = a_r - \sum_j \frac{b_j \Gamma_j e^{i\varphi_j}}{\omega - \omega_j + i\Gamma_j}$$

where a_r is the background amplitude, b_j and φ_j are the amplitudes and phases of each modes, and ω_j and Γ_j are the resonance frequencies and linewidths. The fitting curves match well the experimental data (Fig. 3). Because of the small thickness of the Ag_2O dielectric layer, the plasmonic resonances of the resonators don't shift appreciably in frequency (table 1). However, despite the small thickness, the native silver-oxide layer increases the Q-factor of the dark-mode significantly (27 %), while the Q-factor of the bright-mode is practically unaffected with respect to the Q-factors for the ASRR-Ag sample (see table 1). The increase of the Q-factor of the sub-radiant dark-mode is expected to provide an increase in the near-field absorption. After the AFM and FTIR measurements the arrays were coated with a 200 nm poly-methylmethacrylate (PMMA) layer, which was used to quantify the absorption enhancement in the near-field in the PTIR experiments.

PTIR uses a pulsed wavelength-tunable IR laser to illuminate the sample an AFM tip operating in contact mode as a local detector (Fig. 4) to measure nanoscale IR spectra and maps, thus providing information on the sample chemical composition beyond the diffraction limit of IR light [3, 37, 38, 43-46]. Very recently the PTIR technique was extended to the visible range, allowing acquisition of correlated electronic and vibrational absorption maps and spectra with wavelength independent resolution as high as 20 nm [47]. Notably, the PTIR signal, Fig. 4(b), is proportional to the absorbed energy [37] and it is independent on scattering; consequently the PTIR spectra are directly comparable with far-field IR spectral libraries and allow materials identification in the near-field [48].

Because of the broad applicability of IR spectroscopy and its chemical specificity, PTIR has enabled the characterization of diverse samples including: polymers [49, 50], metal-organic frameworks [51], tri-halide perovskites [52, 53], bacteria [43, 54], cells [55, 56], proteins [57] and drugs nanocrystals [58]. Recently our group applied the PTIR technique to measure high resolution absorption spectra and maps in the near-field surrounding PMMA coated of gold ASRRs which enabled the quantification of the SEIRA absorption enhancement with ≈ 100 nm resolution [3]. For example, asymmetric near-field SEIRA enhancements were measured as a function of the incident illumination direction in resonators due to the angle-dependent interference between the electric and magnetic excitation channels of the resonators' dark-mode [2]. PTIR was also used to measure absorption spectra and maps of the dark-mode in bare ASSR structures [59]. Recently, a modification of the PTIR technique that relies on lasers with tunable wavelength and repetition rate, in combination with the strong electromagnetic field enhancement present in the nanogap between a gold coated tip and a gold coated substrate was used to achieve monolayer sensitivity [60]. A review on nanoscale IR spectroscopy and imaging has been reported recently elsewhere [61].

PTIR experiments were carried out using a commercial PTIR setup that consists of an AFM microscope operating in contact mode and a wavelength tunable (from 2.5 μm to 9.76 μm) pulsed laser. The laser consist of an optical parametric oscillator based on a non-critically phase-matched ZnGeP2 crystal which emits light pulses 10 ns long at 1 kHz repetition rate. A rotating ZnSe wire grid linear polarizer is used as a variable attenuator to control the light intensity and a polarization control module, consisting of three motorized mirrors, is used to obtain the desired polarization at the sample. In the PTIR experiments, the samples were illuminated at

45º by total internal reflection from the prism side, Fig. 4(a). In particular, all the resonators studied in this work were illuminated from the dielectric side at 45° from the short arc side [2] and the light polarization was in the sample plane and in the direction parallel to the long direction of the arcs. The absorption of a laser pulse by a sample induces heating, sample expansion, and mechanical excitation of the AFM cantilever in contact with the sample, Fig. 4(b). Although the laser spot size at the sample is large (≈ 30 μm, Fig. 4(c)), the AFM cantilever provides nanoscale spatial resolution by transducing locally the small sample expansion into large cantilever oscillations that are detected in the far-field by reflecting a diode laser into the AFM four-quadrant detector.

Local infrared spectra were obtained keeping the AFM tip in a fixed location and by plotting the maximum amplitude of the tip deflection (average of 256 pulses) as a function of wavelength (tuned in intervals of 4 cm^{-1}). PTIR spectra of 8 individual hot-spots were measured and averaged to compare the near-field SEIRA enhancements of the two arrays. PTIR images were obtained by plotting the amplitude of the tip deflection as a function of location when scanning the AFM tip under constant wavelength illumination. The acquisition of the AFM topography and PTIR signals was synchronized so that the PTIR signal deriving from 32 laser pulses was averaged during the time necessary to scan over each single AFM topography pixel. A 50 nm × 50 nm pixel size was used for all image acquisitions. Commercially available 450 μm long silicon contact-mode AFM probes with a nominal spring constant between 0.07 N/m and 0.4 N/m were used for this study. The total internal reflection illumination geometry was chosen because it minimizes the direct light-tip interaction without requiring gold coated tips that are otherwise necessary when illuminating the sample from the tip side [60] which may also perturb the plasmonic response of the resonators.

3. Results and discussion

The Figs. 5(a, e) show the AFM height images of the PMMA coated ASRR-Ag and ASRR-Ag-Ag_2O-Ag samples, which allow identifying the position of the resonators structures under the 200 nm thick PMMA layer. The corresponding PTIR images (Figs. 5(b-d) for ASRR-Ag and Figs. 5(f-h) for ASRR-Ag-Ag2O-Ag) show near-field absorption hot-spots in the resonators gaps. The PTIR images were acquired with identical conditions and are displayed in common scale. Since the PTIR signal intensity is proportional to the absorbed energy [37], the PTIR images in Fig. 5 represent the direct image of the local absorption enhancement in the near-field. This is consistent with experiments and the numerical calculations of previous work on similar gold structures [3].

After imaging, the AFM tip was moved to the SEIRA hot-spot locations and PTIR spectra were obtained by sweeping the laser wavelength. Representative PMMA PTIR spectra from the hot-spots are compared in Fig. 6 along with a reference PMMA spectrum. Each PTIR spectrum is the average of the spectra obtained from the 8 hot-spot locations identified in Fig. 5. For each sample, a PTIR spectrum of bare PMMA obtained from a location 300 μm away of the resonators arrays. To take into account sample-to-sample differences in the PMMA thickness, the bare PMMA spectra from ASRR-Ag was used as a reference and the bare PMMA spectrum from the ASRR-Ag-Ag_2O-Ag sample was normalized in its respect (yielding a spectral scaling factor). The spectra were further normalized with respect to the resonator thickness (determined by AFM before coating the arrays with PMMA). Again, the thickness of the ASRR-Ag sample was used as reference. The sample to sample Ag thickness variation was mainly due to the variability of the electron beam deposition process. The near-field SEIRA enhancement measured at 1191 cm^{-1} peak (CH_3 wagging mode) was 6.55 ± 0.63 and 9.40 ± 0.33 with respect to bare PMMA for the ASRR-Ag and for the ASRR-Ag-Ag_2O-Ag samples respectively. Despite the small thickness (≈ 1 nm or 2 nm) of the dielectric layer in ASRR-Ag-Ag_2O-Ag, the enhancement which is the average across the whole PMMA thickness (≈ 200 nm), is ≈ 44 %

larger than for the fully metallic sample. This increase of local near field absorption is consistent with the increase in the resonator's Q-factor in the far-field.

In the M-D-M structure, the dielectric layer (Ag_2O) effectively separates the two metallic silver layers in the vertical direction so that when the resonators are excited, two surface plasmon resonances are produced in the top and bottom layers creating a region of high E-field in the PMMA between the arcs of each ASRRs. In comparison with the fully metallic structure the plasmonic interaction between the two Ag layers in the M-D-M resonators amplifies the plasmonic excitation [29, 31, 33]. A similar enhancing effect was reported by measuring the SERS response of silver films sandwiching a thin silver-oxide layer, which peaked for 48 hours of air exposure between the two silver depositions [29].

4. Conclusion

In summary, Ag-Ag_2O-Ag ASRR structures were fabricated and their spectral response was compared with bare Ag ASRR in both the far-field and the near-field. Results show that the thin Ag_2O dielectric layer sandwiched between two silver layers increases the quality factor of the resonators dark-mode. The PTIR technique was utilized to image the resonators' hot-spots and to obtain local enhanced absorption spectra that were used to quantify the near-field SEIRA enhancements surrounding the plasmonic nanostructures with approximately 100 nm resolution. The near-field results show that the thin ($\approx$ 1 nm) dielectric layer in the M-D-M structure provides a 44 % increase in the local SEIRA enhancement in a PMMA layer coated resonators when compared to the entirely Ag resonators of the same size and shape. We speculate that the dielectric layer may provide both extreme electric field confinement (up to $\approx \lambda/8600$) close to the dielectric layer and may enable a synergistic excitation of the plasmonic modes of the two metallic layers. The natural oxidation of silver in air is a very simple and cheap method to increase the performance of silver plasmonic resonators. While the absorption coefficient of the fabricated dielectric layers in this work is unknown, a dielectric layer with a small absorption coefficient should be advantageous for reducing the losses which otherwise would occurs in the fully metallic layer. Because our approach combines two common strategies for increasing the quality factors of plasmonic nanostructures: the excitation of a resonator dark-modes and the metal-dielectric-metal structure, it should be of general applicability and we believe it may help in boosting the performance of plasmonic nanomaterials in applications relying enhanced light-matter interaction [62] at the nanoscale such as sensing [5], therapeutics [63, 64] and energy [7].

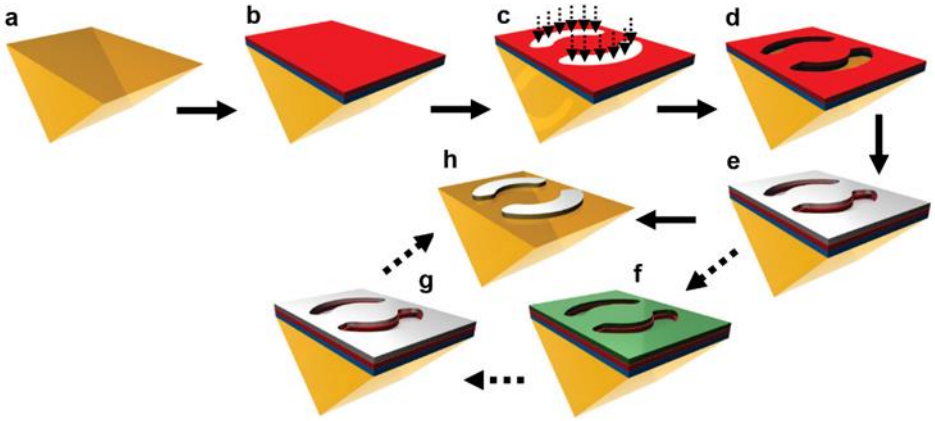

Fig. 1. Nanofabrication scheme: a) ZnSe right angle prisms were cleaned in an ultrasonic bath with acetone (1 min) and isopropyl alcohol (1 min) followed by oxygen plasma cleaning (15 min) before the ASRRs fabrication. b) a PMMA bilayer (250 nm and 300 nm) positive electron beam resist was spun (25 Hz) on the ZnSe prism and cured (140 °C for 15 min and 30 min respectively) before depositing an aluminum charge dissipation layer (30 nm ± 5 nm) with an electron-beam evaporator. c) the resonator arrays (200 μm x 200 μm) were written with electron beam lithography (100 kV accelerating voltage, 1000 μC/cm^2 electron beam dose). The aluminum layer was then removed using an aqueous tetramethylammonium hydroxide (2.4 % volume fraction) solution. d) The pattern was developed with a mixture of methyl isobutylketone and isopropyl alcohol e) electron beam deposition was used to deposit a 5 nm chromium adhesion layer and a silver layer (≈ 170 nm for ARRS-Ag or ≈ 85 nm for ASRR-Ag-Ag_2O-Ag), f) In the case of ASRR-Ag-Ag_2O-Ag (dotted arrows), a thin dielectric layer (green) is grown in air, g) In the case of ASRR-Ag-Ag_2O-Ag the M-D-M structure is obtained by electron beam deposition of a second (≈ 85 nm thick) silver layer, h) The resonators arrays are obtained after lift of in N-methyl-2-pyrrolidone PMMA remover.

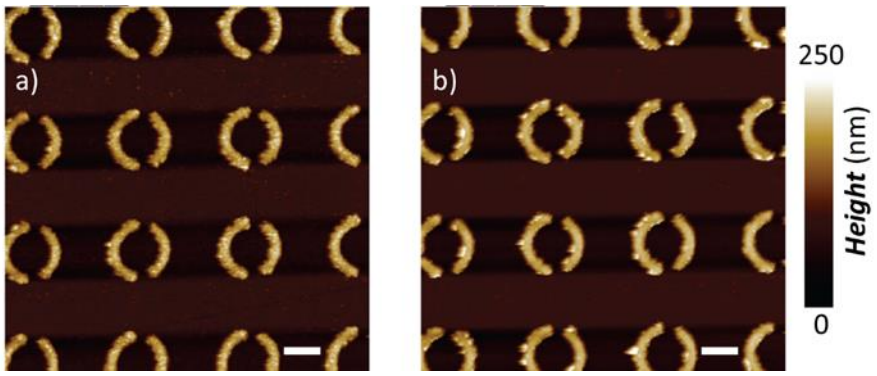

Fig. 2. AFM images of ASRR-Ag (a) and ASRR-Ag-Ag_2O-Ag (b) arrays All scale bars are 1 μm.

Table 1: Geometrical dimensions of the ASRR samples as measured by AFM and characteristic of the plasmon resonant frequency in those devices as measured by FTIR. The uncertainties in the resonator dimensions represent a single standard deviation in the measurements on nominally identical devices. The uncertainty in the plasmon resonant frequency and Q factor represent a single standard deviation from Fano interference fitting of FTIR resonance peak.

Sample	ASRR-Ag	ASRR-Ag-Ag_2O-Ag
Diameter (nm)	1731 ± 30	1750 ± 33
Pitch (nm)	3023 ± 31	3050 ± 58
Thickness (nm)	174 ± 8	166 ± 3
Strip width (nm)	335 ± 28	351 ± 38
Resonance frequency (cm^{-1}) (bright mode)	1477 ± 2	1459 ± 2
Resonance frequency (cm^{-1}) (dark mode)	1186 ± 0.5	1179 ± 0.5
Q-factor (bright mode)	3.21 ± 0.05	3.17 ± 0.05
Q-factor (dark mode)	12.93 ± 0.10	16.45 ± 0.11

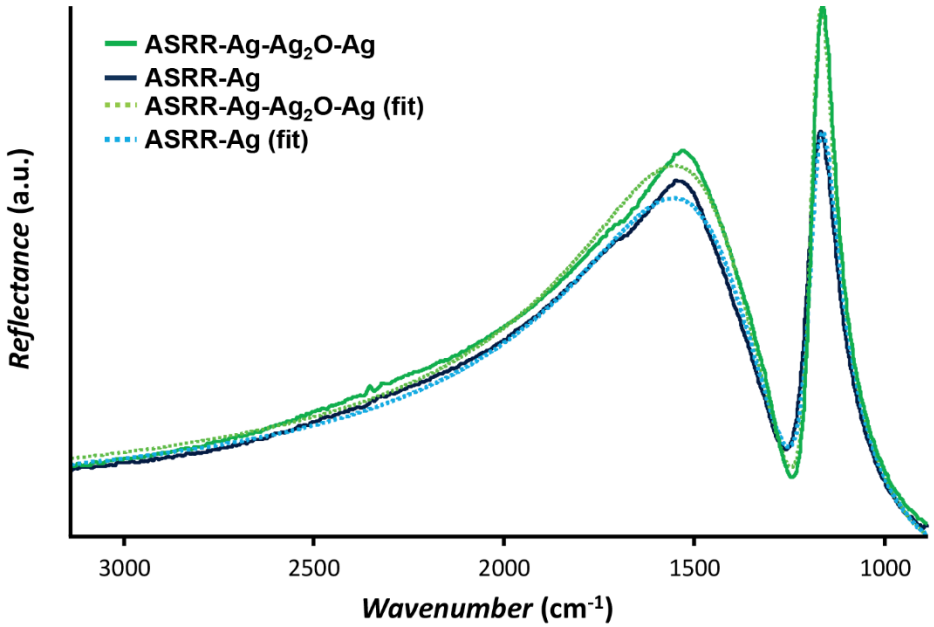

Fig. 3. Far-field FTIR reflection spectra of ASRR-Ag (dark blue) and ASRR-Ag-Ag_2O-Ag (dark green); both arrays show plasmonic peaks with the characteristic Fano-distortion in the same spectral region. The spectra are displayed with a common intensity scale. The fitting curves using the Fano-interference model are drawn with dotted lines for ASRR-Ag (light blue) and ASRR-AgO-Ag (light green).

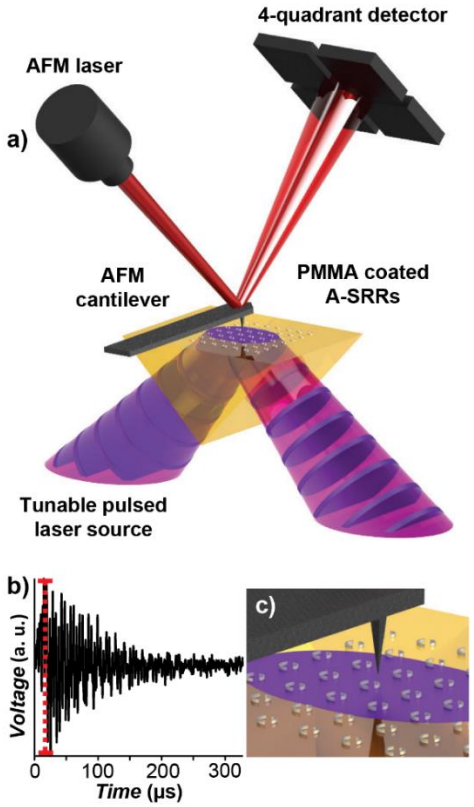

Fig. 4. a) Schematic of the PTIR measurement. When IR laser pulses (purple) are absorbed by the sample (PMMA coating A-SRRs) it expands deflecting the AFM cantilever. The deflection amplitude is proportional to the absorbed energy and it is measured by the AFM four-quadrant detector on a time scale much faster than the AFM feedback. b) The PTIR signal is defined by the maximum of the peak to peak deflection during the cantilever ring down. c) The laser is focused under the AFM tip to a spot of ≈ 30 μm in diameter. The tip is used to extract local IR spectra and maps. The total internal reflection geometry minimizes the light-tip direct interaction.

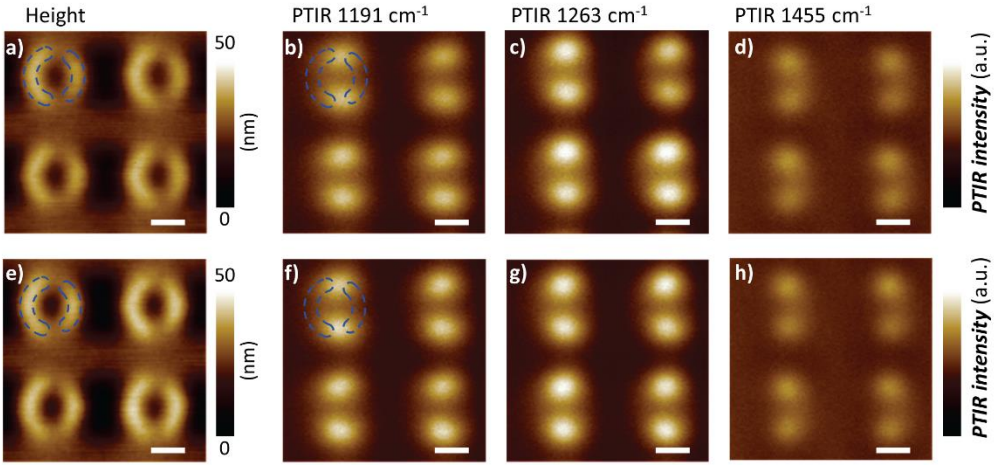

Fig. 5. a) AFM image of PMMA coated ASRR-Ag. b, c, d) PTIR images obtained in correspondence of PMMA absorption peaks: b) CH_3 wagging mode at 1191 cm^{-1} (8.40 µm), c) C-O stretching mode at 1263 cm^{-1} (7.92 µm) and d), CH_3 antisymmetric deformation mode at 1455 cm^{-1} (6.87 µm). e) AFM image of PMMA coated ASRR-Ag-Ag_2O-Ag. f, g, h) PTIR images obtained in correspondence of PMMA absorption peaks: f) CH_3 wagging mode at 1191 cm^{-1} (8.40 µm), g) C-O stretching mode at 1263 cm^{-1} (7.92 µm) and h), CH_3 antisymmetric deformation mode at 1455 cm^{-1} (6.87 µm). The blue dotted lines schematically outline the embedded resonators. Hot-spots corresponding to the regions of enhanced absorption are observed in the gaps between the resonators arcs. A common intensity scale is shared across all PTIR images. All scale bars are 1 µm. The intensities of the PTIR images of the two samples are not normalized with respect to the PMMA nor Ag thickness as described in main text for the PTIR spectra.

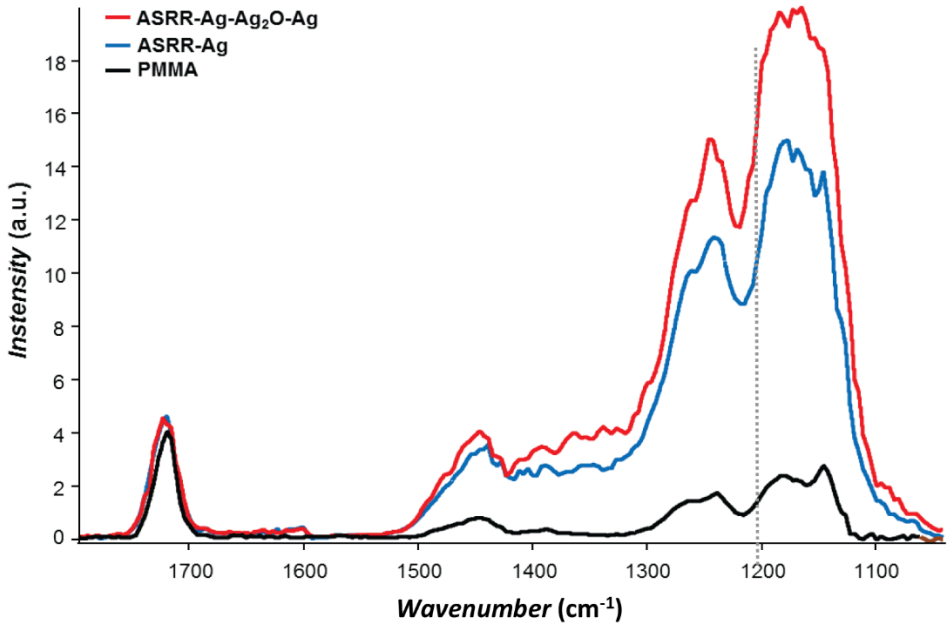

Fig. 6. The normalized PTIR spectra obtained from the SEIRA hot-spots locations for ASRR-Ag (blue), ASRR-Ag-Ag_2O-Ag (red), are compared with the PTIR spectrum of the bare PMMA reference film measured in proximity of the ASSR-Ag reference array (black). PTIR spectra for each sample were averaged over 8 hot-spot locations and displayed in common intensity scale. Each spectrum was scaled with respect to the relative intensity of the bare PMMA spectra in each dataset and with respect to the Ag thickness of the resonators as described in the main text. The vertical dotted line mark the spectral position at which the near-field SEIRA enhancement was quantified.

References

1. D. Smith, J. Pendry, and M. Wiltshire, "Metamaterials and negative refractive index," Science **305**, 788-792 (2004).
2. V. Aksyuk, B. Lahiri, G. Holland, and A. Centrone, "Near-field asymmetries in plasmonic resonators," Nanoscale **7**, 3634-3644 (2015).
3. B. Lahiri, G. Holland, V. Aksyuk, and A. Centrone, "Nanoscale imaging of plasmonic hot spots and dark modes with the photothermal-induced resonance technique," Nano Lett. **13**, 3218-3224 (2013).
4. E. Cubukcu, S. Zhang, Y.-S. Park, G. Bartal, and X. Zhang, "Split ring resonator sensors for infrared detection of single molecular monolayers," Appl. Phys. Lett. **95**, 043113 (2009).
5. R. Adato, A. A. Yanik, J. J. Amsden, D. L. Kaplan, F. G. Omenetto, M. K. Hong, S. Erramilli, and H. Altug, "Ultra-sensitive vibrational spectroscopy of protein monolayers with plasmonic nanoantenna arrays," Proc. Natl. Acad. Sci. U. S. A. **106**, 19227-19232 (2009).
6. A. J. Morfa, K. L. Rowlen, T. H. Reilly, M. J. Romero, and J. van de Lagemaat, "Plasmon-enhanced solar energy conversion in organic bulk heterojunction photovoltaics," Appl. Phys. Lett. **92**, 013504 (2008).

7. H. A. Atwater, and A. Polman, "Plasmonics for improved photovoltaic devices," Nat. Mater. **9**, 205-213 (2010).
8. D. Schurig, J. Mock, B. Justice, S. Cummer, J. Pendry, A. Starr, and D. Smith, "Metamaterial electromagnetic cloak at microwave frequencies," Science **314**, 977-980 (2006).
9. C. Enkrich, M. Wegener, S. Linden, S. Burger, L. Zschiedrich, F. Schmidt, J. Zhou, T. Koschny, and C. Soukoulis, "Magnetic metamaterials at telecommunication and visible frequencies," Phys. Rev. Lett. **95**, 203901 (2005).
10. S. Linden, C. Enkrich, M. Wegener, J. Zhou, T. Koschny, and C. M. Soukoulis, "Magnetic response of metamaterials at 100 terahertz," Science **306**, 1351-1353 (2004).
11. V. M. Shalaev, "Optical negative-index metamaterials," Nat. Photonics **1**, 41-48 (2007).
12. J. Zhou, T. Koschny, M. Kafesaki, E. Economou, J. Pendry, and C. Soukoulis, "Saturation of the magnetic response of split-ring resonators at optical frequencies," Phys. Rev. Lett. **95**, 223902 (2005).
13. B. Lahiri, A. Z. Khokhar, R. M. De La Rue, S. G. McMeekin, and N. P. Johnson, "Asymmetric split ring resonators for optical sensing of organic materials," Opt. Express **17**, 1107-1115 (2009).
14. B. Lahiri, S. G. McMeekin, A. Z. Khokhar, R. M. De La Rue, and N. P. Johnson, "Magnetic response of split ring resonators (SRRs) at visible frequencies," Opt. Express **18**, 3210-3218 (2010).
15. F. Le, D. W. Brandl, Y. A. Urzhumov, H. Wang, J. Kundu, N. J. Halas, J. Aizpurua, and P. Nordlander, "Metallic nanoparticle arrays: a common substrate for both surface-enhanced Raman scattering and surface-enhanced infrared absorption," ACS Nano **2**, 707-718 (2008).
16. A. Pucci, F. Neubrech, D. Weber, S. Hong, T. Toury, and M. L. de la Chapelle, "Surface enhanced infrared spectroscopy using gold nanoantennas," Phys. Status Solidi B **247**, 2071-2074 (2010).
17. K. Chen, R. Adato, and H. Altug, "Dual-band perfect absorber for multispectral plasmon-enhanced infrared spectroscopy," ACS Nano **6**, 7998-8006 (2012).
18. H. Aouani, H. Sipova, M. Rahmani, M. Navarro-Cia, K. Hegnerova, J. Homola, M. H. Hong, and S. A. Maier, "Ultrasensitive broadband probing of molecular vibrational modes with multifrequency optical antennas," ACS Nano **7**, 669-675 (2013).
19. F. Neubrech, A. Pucci, T. W. Cornelius, S. Karim, A. Garcia-Etxarri, and J. Aizpurua, "Resonant plasmonic and vibrational coupling in a tailored nanoantenna for infrared detection," Phys. Rev. Lett. **101**, 157403 (2008).
20. C. H. Wu, A. B. Khanikaev, R. Adato, N. Arju, A. A. Yanik, H. Altug, and G. Shvets, "Fano-resonant asymmetric metamaterials for ultrasensitive spectroscopy and identification of molecular monolayers," Nat. Mater. **11**, 69-75 (2012).
21. R. Bukasov, and J. S. Shumaker-Parry, "Silver nanocrescents with infrared plasmonic properties as tunable substrates for surface enhanced infrared absorption spectroscopy," Anal. Chem. **81**, 4531-4535 (2009).
22. C. Huck, F. Neubrech, J. Vogt, A. Toma, D. Gerbert, J. Katzmann, T. Härtling, and A. Pucci, "Surface-enhanced infrared spectroscopy using nanometer-sized gaps," ACS Nano **8**, 4908-4914 (2014).
23. M. Abb, Y. Wang, N. Papasimakis, C. H. de Groot, and O. L. Muskens, "Surface-enhanced infrared spectroscopy using metal oxide plasmonic antenna arrays," Nano Lett. **14**, 346-352 (2014).
24. M. I. Stockman, "Nanoplasmonics: The physics behind the applications," Phys. Today **64**, 39-44 (2011).

25. V. Fedotov, M. Rose, S. Prosvirnin, N. Papasimakis, and N. Zheludev, "Sharp trapped-mode resonances in planar metamaterials with a broken structural symmetry," Phys. Rev. Lett. **99**, 147401 (2007).
26. B. Lahiri, S. G. McMeekin, R. M. De La Rue, and N. P. Johnson, "Enhanced Fano resonance of organic material films deposited on arrays of asymmetric split-ring resonators (A-SRRs)," Opt. Express **21**, 9343-9352 (2013).
27. C. Debus, and P. H. Bolivar, "Frequency selective surfaces for high sensitivity terahertz sensing," Appl. Phys. Lett. **91**, 184102 (2007).
28. K. Aydin, I. M. Pryce, and H. A. Atwater, "Symmetry breaking and strong coupling in planar optical metamaterials," Opt. Express **18**, 13407-13417 (2010).
29. H. Li, and B. M. Cullum, "Dual layer and multilayer enhancements from silver film over nanostructured surface-enhanced Raman substrates," Appl. Spectrosc. **59**, 410-417 (2005).
30. J. Luo, X. Y. Zhuang, W. Xiong, and J. Yao, "Numerical study on optical properties of Ag/SiO2SiO2/Ag sandwich nanocrescents substrate," J. Mod. Opt. **59**, 1316-1321 (2012).
31. L. Yang, C. Du, and X. Luo, "Numerical study of optical properties of Ag/SiO2/Ag sandwich nanobowties," J. Comput. Theor. Nanosci. **6**, 106-111 (2009).
32. D. Dey, J. Kohoutek, R. M. Gelfand, A. Bonakdar, and H. Mohseni, "Quantum-cascade laser integrated with a metal-dielectric-metal-based plasmonic antenna," Opt. Lett. **35**, 2783-2785 (2010).
33. M. L. Wan, H. J. Du, Y. L. Song, and F. Q. Zhou, "Tunable localized surface plasmon resonances of asymmetric Au/SiO2/Au cross-shape nanobars," Mod. Phys. Lett. B **28** (2014).
34. C. M. Soukoulis, and M. Wegener, "Past achievements and future challenges in the development of three-dimensional photonic metamaterials," Nat. Photonics **5**, 523-530 (2011).
35. V. M. Shalaev, W. Cai, U. K. Chettiar, H.-K. Yuan, A. K. Sarychev, V. P. Drachev, and A. V. Kildishev, "Negative index of refraction in optical metamaterials," Opt. Lett. **30**, 3356-3358 (2005).
36. T. Xu, A. Agrawal, M. Abashin, K. J. Chau, and H. J. Lezec, "All-angle negative refraction and active flat lensing of ultraviolet light," Nature **497**, 470-474 (2013).
37. B. Lahiri, G. Holland, and A. Centrone, "Chemical imaging beyond the diffraction limit: experimental validation of the PTIR technique," Small **9**, 439-445 (2013).
38. A. Dazzi, R. Prazeres, E. Glotin, and J. M. Ortega, "Local infrared microspectroscopy with subwavelength spatial resolution with an atomic force microscope tip used as a photothermal sensor," Opt. Lett. **30**, 2388-2390 (2005).
39. A. Derooij, "The Oxidation of silver by atomic oxygen," Esa J-Eur. Space Agen. **13**, 363-382 (1989).
40. T. W. H. Oates, M. Losurdo, S. Noda, and K. Hinrichs, "The effect of atmospheric tarnishing on the optical and structural properties of silver nanoparticles," J. Phys. D App. Phys. **46** (2013).
41. F. Hao, P. Nordlander, Y. Sonnefraud, P. V. Dorpe, and S. A. Maier, "Tunability of subradiant dipolar and Fano-type plasmon resonances in metallic ring/disk cavities: implications for nanoscale optical sensing," ACS Nano **3**, 643-652 (2009).
42. N. Verellen, P. Van Dorpe, C. Huang, K. Lodewijks, G. A. E. Vandenbosch, L. Lagae, and V. V. Moshchalkov, "Plasmon line shaping using nanocrosses for high sensitivity localized surface plasmon resonance sensing," Nano Lett. **11**, 391-397 (2011).
43. A. Dazzi, R. Prazeres, F. Glotin, J. M. Ortega, M. Al-Sawaftah, and M. de Frutos, "Chemical mapping of the distribution of viruses into infected bacteria with a photothermal method," Ultramicroscopy **108**, 635-641 (2008).

44. A. Dazzi, C. B. Prater, Q. C. Hu, D. B. Chase, J. F. Rabolt, and C. Marcott, "AFM-IR: combining atomic force microscopy and infrared spectroscopy for nanoscale chemical characterization," Appl. Spectrosc. **66**, 1365-1384 (2012).
45. A. M. Katzenmeyer, V. Aksyuk, and A. Centrone, "Nanoscale infrared spectroscopy: improving the spectral range of the photothermal induced resonance technique," Anal. Chem. **85**, 1972-1979 (2013).
46. G. Ramer, A. Balbekova, A. Schwaighofer, and B. Lendl, "Method for time-resolved monitoring of a solid state biological film using photothermal infrared nanoscopy on the example of poly-L-lysine," Anal. Chem. **87**, 4415-4420 (2015).
47. A. M. Katzenmeyer, G. Holland, K. Kjoller, and A. Centrone, "Absorption spectroscopy and imaging from the visible through mid-infrared with 20 nm resolution," Anal. Chem. **87**, 3154-3159 (2015).
48. C. Marcott, M. Lo, K. Kjoller, C. Prater, and I. Noda, "Spatial differentiation of sub-micrometer domains in a poly(hydroxyalkanoate) copolymer using instrumentation that combines atomic force microscopy (AFM) and infrared (IR) spectroscopy," Appl. Spectrosc. **65**, 1145-1150 (2011).
49. J. R. Felts, K. Kjoller, M. Lo, C. B. Prater, and W. P. King, "Nanometer-scale infrared spectroscopy of heterogeneous polymer nanostructures fabricated by tip-based nanofabrication," ACS Nano **6**, 8015-8021 (2012).
50. Z. Cui, C. Coletta, A. Dazzi, P. Lefrancois, M. Gervais, S. Néron, and S. Remita, "radiolytic method as a novel approach for the synthesis of nanostructured conducting polypyrrole," Langmuir **30**, 14086-14094 (2014).
51. A. M. Katzenmeyer, J. Canivet, G. Holland, D. Farrusseng, and A. Centrone, "Assessing chemical heterogeneity at the nanoscale in mixed-ligand metal-organic frameworks with the PTIR technique," Angew. Chem. Int. Ed. **53**, 2852-2856 (2014).
52. R. Dong, Y. Fang, J. Chae, J. Dai, Z. Xiao, Q. Dong, Y. Yuan, A. Centrone, X. C. Zeng, and J. Huang, "High-gain and low-driving-voltage photodetectors based on organolead triiodide perovskites," Adv. Mater. **27**, 1912-1918 (2015).
53. Y. Yuan, J. Chae, Y. Shao, Q. Wang, Z. Xiao, A. Centrone, and J. Huang, "Photovoltaic switching mechanism in lateral structure hybrid perovskite solar cells," Adv. Energy Mater. **5**, 1500615 (2015).
54. A. Deniset-Besseau, C. B. Prater, M. J. Virolle, and A. Dazzi, "Monitoring triacylglycerols accumulation by atomic force microscopy based infrared spectroscopy in streptomyces species for biodiesel applications," J. Phys. Chem. Lett. **5**, 654-658 (2014).
55. C. Mayet, A. Dazzi, R. Prazeres, E. Allot, E. Glotin, and J. M. Ortega, "Sub-100 nm IR spectromicroscopy of living cells," Opt. Lett. **33**, 1611-1613 (2008).
56. E. Kennedy, R. Al-Majmaie, M. Al-Rubeai, D. Zerulla, and J. H. Rice, "Nanoscale infrared absorption imaging permits non-destructive intracellular photosensitizer localization for subcellular uptake analysis," Rsc Advances **3**, 13789-13795 (2013).
57. T. Muller, F. S. Ruggeri, A. J. Kulik, U. Shimanovich, T. O. Mason, T. P. J. Knowles, and G. Dietler, "Nanoscale spatially resolved infrared spectra from single microdroplets," Lab Chip **14**, 1315-1319 (2014).
58. A. J. Harrison, E. A. Bilgili, S. P. Beaudoin, and L. S. Tayor, "Atomic force microscope infrared spectroscopy of griseofulvin nanocrystals," Anal. Chem. **85**, 11449-11455 (2013).
59. A. M. Katzenmeyer, J. Chae, R. Kasica, G. Holland, B. Lahiri, and A. Centrone, "Nanoscale imaging and spectroscopy of plasmonic modes with the PTIR technique," Adv. Optical Mater. **2**, 718-722 (2014).
60. F. Lu, M. Z. Jin, and M. A. Belkin, "Tip-enhanced infrared nanospectroscopy via molecular expansion force detection," Nat. Photonics **8**, 307-312 (2014).
61. A. Centrone, "Infrared imaging and spectroscopy beyond the diffraction limit," Annu. Rev. Anal. Chem. **8**, 101-126 (2015).

62. R. Stanley, "Plasmonics in the mid-infrared," Nat. Photonics **6**, 409-411 (2012).
63. J. H. Park, G. von Maltzahn, L. L. Ong, A. Centrone, T. A. Hatton, E. Ruoslahti, S. N. Bhatia, and M. J. Sailor, "Cooperative nanoparticles for tumor detection and photothermally triggered drug delivery," Adv. Mater. **22**, 880-885 (2010).
64. G. von Maltzahn, A. Centrone, J. H. Park, R. Ramanathan, M. J. Sailor, T. A. Hatton, and S. N. Bhatia, "SERS-coded gold nanorods as a multifunctional platform for densely multiplexed near-infrared imaging and photothermal heating," Adv. Mater. **21**, 3175-3180 (2009).